How climate, migration ability and habitat fragmentation affect the projected future distribution of European beech?

Frédérik Saltré, Anne Duputié, Cédric Gaucherel, & Isabelle Chuine

1. Parameterisation of PHENOFIT in this study

Phenological sub-models of PHENOFIT determining the dates of budburst, flowering, fructification and leaf senescence) are parameterized using time-series observations of phenological events in natural populations, and the daily temperatures of the nearest meteorological station (within 10 km and within 200 m altitude of the corresponding phenological observation station). Parameter optimization is carried through minimizing the residual sum of squares, using a simulated annealing algorithm (Chuine *et al.*, 1998). Budburst date was best described using a Unimodal model to describe the accumulation of chilling units during endodormancy, and a Sigmoid model to describe the accumulation of forcing units during ecodormancy (Chuine *et al.*, 2013). Because beech buds are compound, the flowering model only differed from the budburst model by the number of forcing units needed to achieve flowering. Fructification was described using the model described in Chuine and Beaubien (2001), and leaf senescence using the model by Delpierre et al. (2009).

For budburst date, flowering date and leaf senescence date, different models were fitted from nine populations covering most of the range of environmental conditions where beech naturally occurs (Fig S1). Because accurate observations of the date of fructification were missing from most of the range, only one model was fitted for the date of fructification (Fig S1). Phenological observations were retrieved from the French and from the European phenological databases (PEP, http://www.pep725.eu/ and Observatoire des Saisons, http://www.gdr2968.cnrs.fr, all observations were more recent than 1974), and daily meteorological records for the corresponding time period and the closest meteorological station were retrieved from the National Climatic Data Center (http://www.ncdc.noaa.gov/cgi-bin/res40.pl?page=climvisgsod.html) and Météo-France (http://publitheque.meteo.fr/okapi/accueil/okapiWebPubli/index.jsp).

Parameters for the submodels describing resistance to drought and water stress were derived from the literature (http://agriculture.gouv.fr/IMG/pdf/hetre_nov07.pdf), with only one parameter set for the whole range. PHENOFIT was then run for each of the nine parameter sets (differing only by the models determining budburst, flowering and leaf senescence dates), thus yielding nine possible values for fitness for each pixel and each year. In order to account for local adaptation, we then weighted these nine outputs, for each pixel and each year, by the inverse of the pixel's distance to the barycenter of the closest three regions used for calibration:

$$fitness_{pix,year} = \frac{\sum_R \left(fitness_{pix,year,R} / d_{pix,R} \right)}{\sum_R \left(1 / d_{pix,R} \right)}$$
(1)

where $fitness_{pix,year,R}$ is the fitness inferred for the pixel using the model calibrated on region R, $d_{pix,R}$ the distance (in km) to the barycenter of region R, and R corresponds to the closest three calibration regions. Since $fitness_{pix,year,R}$ is bound by [0,1], so is $fitness_{pix,year}$. Since the value for fitness computed over a year varies from a year to the next, final PHENOFIT output ($fitness_{pix}$) was computed as the arithmetic average of yearly fitness over 20 years.

We then determined a threshold for $fitness_{pix}$, below which the species was deemed as "absent". This threshold was chosen to maximize the sum of sensitivity (proportion of correctly identified actual positives) and specificity (proportion of correctly identified negatives), with respect to a consensual map of beech

presence in Europe and amounted to 0.167. The consensual map for beech presence corresponded to the spatial joining of beech occurrences, as provided by five sources of data, all of them relying on international collaborative efforts and with continental coverage: Atlas Flora Europaea (Jalas & Suominen, 1964-2010 ; Lahti & Lampinen, 1999 ; http://www.luomus.fi/english/botany/afe/index.htm), EUFORGEN database (http://www.euforgen.org/distribution_maps.html), JRC database (http://forest.jrc.ec.europa.eu/), EuroVegMap (Bohn et al., 2004; http://www.floraweb.de/vegetation/dnld_eurovegmap.html), and ICP forest plots (http://www.icp-forests.org/). Beech was deemed absent from pixels for which none of these sources of data indicated the species was present.
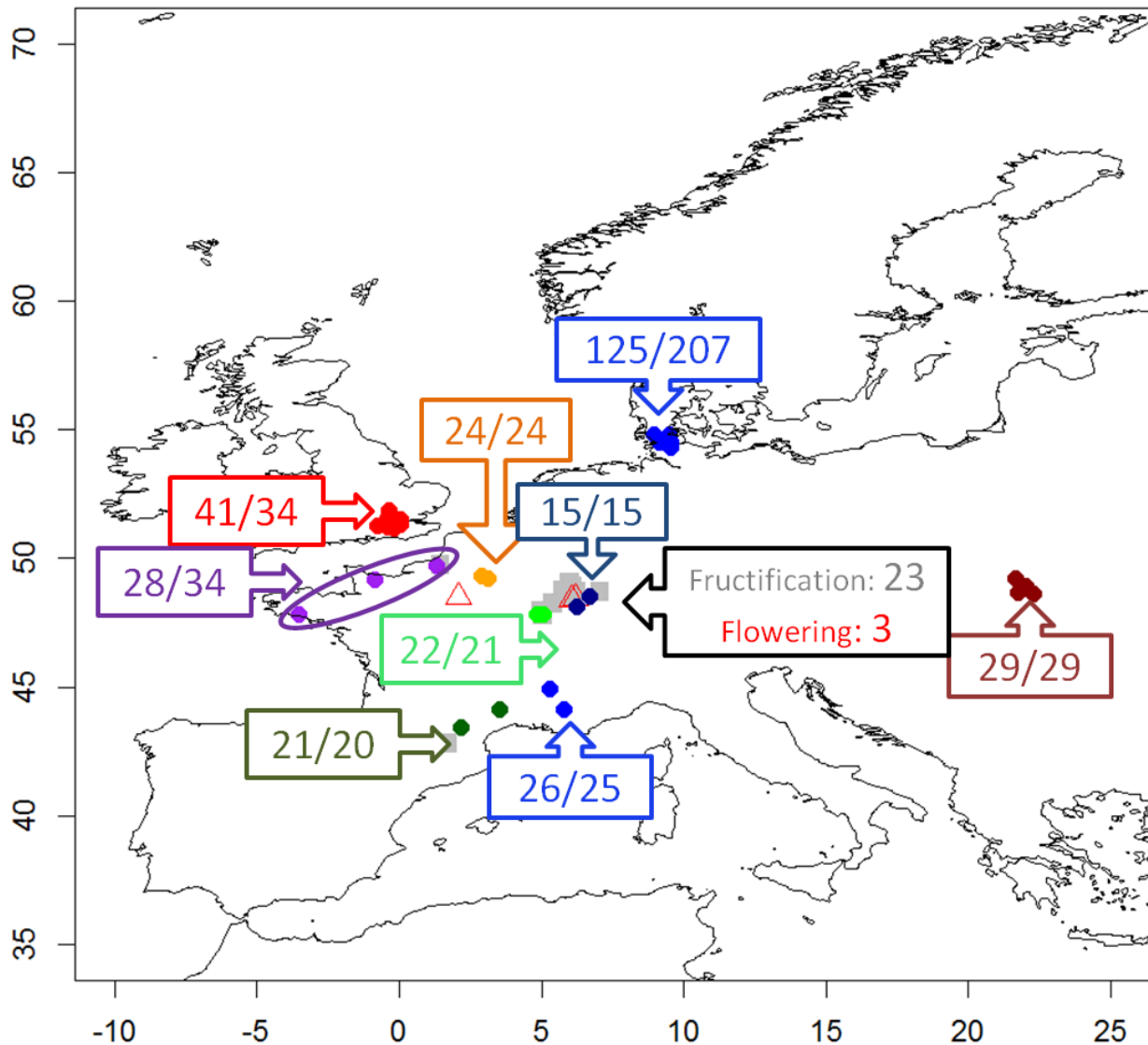
Figure S1. Sites used to parameterize the budburst and leaf senescence date models (circles, colors indicate the nine provenance regions), the flowering date model (red triangles) and the fructification date model (grey squares). For budburst and leaf senescence dates, each color corresponds to one region with specific parameters. Numbers indicate the number of points (location x year) used to calibrate the budburst/leaf senescence models.

2. Coupling PHENOFIT and the Gibbs-based model
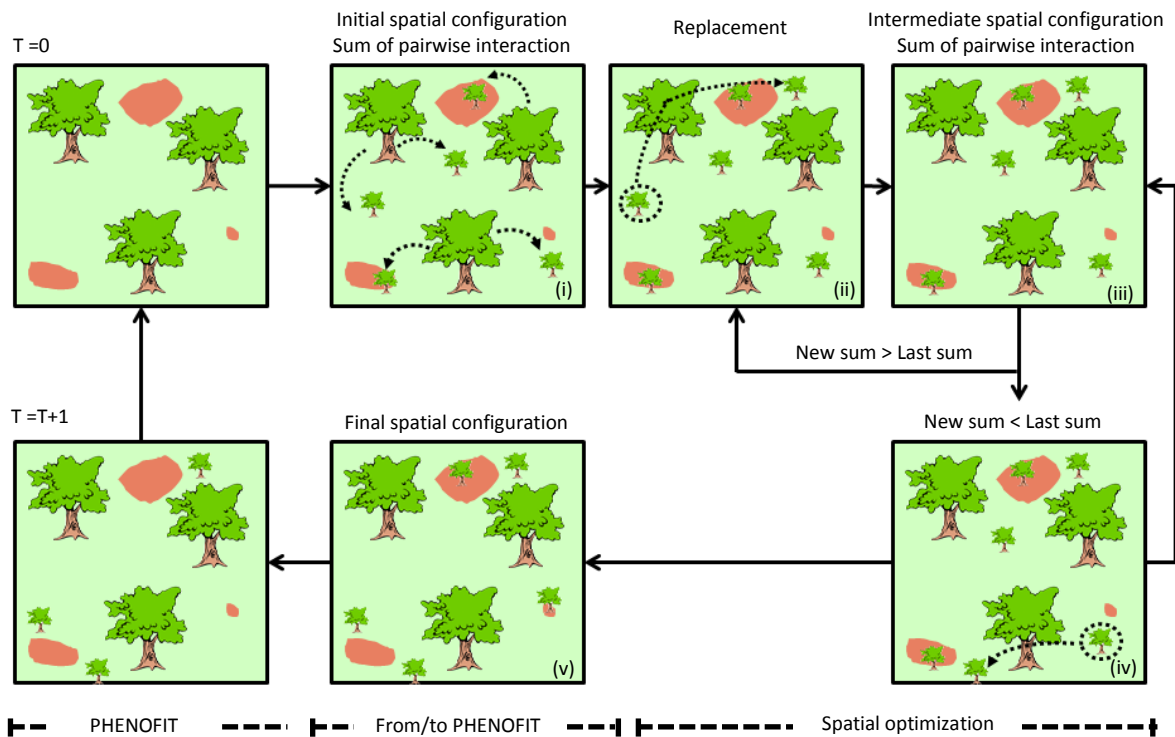
Figure S2. Conceptual scheme of the Gibbs-based migration model coupled with PHENOFIT. The initial spatial configuration of offspring is progressively reorganized as a function of their parents and neighbours until the final spatial configuration characterizing the given species is reached. PHENOFIT simulates suitable (green) or unsuitable (red) habitats and provides the amount of offspring at each time step (Saltré *et al.*, 2013).

Using a discrete time step, the model simulates migration by placing the offspring as a function of the position of the existing trees such that the inherent spatial pattern of the given species (patch, regular or random distribution of individuals observed on field) is reproduced. (i) Offspring are first randomly placed all at once, everywhere on the landscape and the sum of all pairwise interactions between all trees of this initial pattern is calculated. (ii) The position of each offspring is then randomly modified and (iii) the sum of all pairwise interactions of this new pattern is calculated. If the new sum is lower than the former one, the new pattern is adopted; (iv) the position of another offspring is modified and step (iii) proceeds again. If the sum is higher than the former one, the algorithm goes back to the former pattern (ii), the position of another offspring is modified and (ii) a new sum of all pairwise interactions is calculated. The position of replacement of offspring (step ii) is randomly chosen within a region defined by a radius from a parent (i.e. α, defined by the parameterization of the IPF). The optimization is stopped when a certain number of successive iterations fail (empirically optimized it at 10000) to decrease the sum of all interactions. The relocation of offspring thus generates a progressive reorganization of the spatial pattern (v) to reach in the end the spatial pattern of the species. The probability of establishment of a cohort into a grid cell is also constraint by slope, i.e. the first derivative of the average elevation on each grid cell, as follows:

$$P_{i,j} = 1 - \left(\frac{S_{i,j}}{max_{i,j}(S)} \right)$$

With the probability of establishment (P) in a grid cell of coordinate (i, j), the slope (S). An increasing slope decreases the probability of establishment. Individuals placed in unsuitable areas then die. The amount of offspring depends on both the reproduction rate (every 3 years) and the sexual maturity of beech (45 years, Ellenberg 1996). The initial set of cohorts used for the starting of simulations is randomly aged between the age at maturation and the maximal age for beech (i.e. 45-300 years old).

3. The Gibbs' interaction potential function (IPF)

The general form of the non-homogeneous Gibbs process is summarized by the probability f of establishment of an element depending on positions of other individuals (Stoyan & Stoyan, 1998):

$$f(x_1, \ldots, x_n) = K\exp^{\left(-\Sigma_{i<j}\,\varphi(\|x_i-x_j\|)\right)} \prod_{i=1}^{n} p(x_i) \tag{2}$$

where K is a positive normalization constant, $\|x_i - x_j\|$ is the distance between the pair of elements and, $p(\cdot)$ is a non-negative function [$p(x_i) = \hat{\lambda}(x_i)$, where $\hat{\lambda}(\cdot)$ is the estimated intensity function (Illian *et al.*, 2008) proportional to the point density at the location x_i, (Diggle, 1985)], which makes it possible to model trends in the point density, φ is the potential of interaction function (IPF).

The IPF parameterization is the same as in Saltré *et al.,* (2013) and gives both φ and $\|x_i - x_j\|$ values for even-aged tree individuals of a fully mapped 0.4 km² unmanaged pure beech stand located in the north-eastern Italian pre-Alps (46°02'N, 12°25'E, on the Cansiglio's Karst Plateau) such as:

$$\varphi(\|x_i - x_j\|) = \begin{cases} -1.4, & > 0\,\text{m} & \leq & 2\,\text{m} \\ -2.4, & 2\,\text{m} > & \leq & 7\,\text{m} \\ -8.9, & \text{if} & 7\,\text{m} > & \|x_i - x_j\| & \leq & 18\,\text{m} \\ -3.4, & 18\,\text{m} > & \leq & 26\,\text{m} \\ -1.4, & 26\,\text{m} > & \leq & 200\,\text{m} \\ 0, & & > & 200\,\text{m} \end{cases} \tag{3}$$

Because computational constraints limit the maximal number of tree simulated throughout the entire Europe over the next century and tree interactions are only captured until 200 m, which might be too short a distance to account for some long distance migration events, we artificially extended the dataset to calibrate a new IPF for tree cohorts on an artificial 25 km² pure beech stand with the same spatial patterns as the 0.4 km² stand. The IPF parameter sets for tree cohorts are:

$$\varphi(\|x_i - x_j\|) = \begin{cases} -60, & > 0\,\text{m} & \leq & 75\,\text{m} \\ -30, & 75\,\text{m} > & \leq & 250\,\text{m} \\ 10, & \text{if} & 250\,\text{m} > & \|x_i - x_j\| & \leq & 1000\,\text{m} \\ -80, & 1000\,\text{m} > & \leq & 1500\,\text{m} \\ -90, & 1500\,\text{m} > & \leq & 3000\,\text{m} \\ 0, & & > & 3000\,\text{m} \end{cases} \tag{4}$$

a.

b.
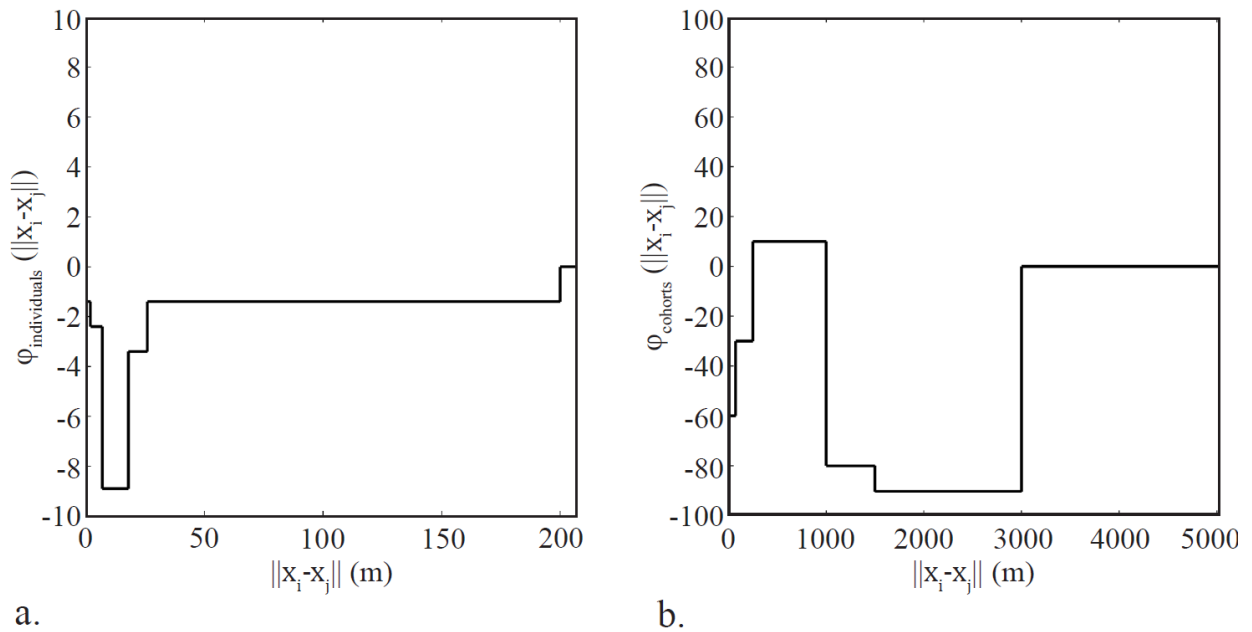
Figure S3. Interaction potential function (IPF) parameterized at individual scale **(a.)** and at cohort scale **(b.).** IPF expresses the pairwise interaction (φ) between elements (individuals or cohorts) as a function of the distance between each other$\|x_i - x_j\|$. As the sum of all interaction over the entire landscape has to be minimized to accurately reproduce the inherent spatial pattern of a given species, the optimal distance between pairs of elements is associated with negative. Due to dataset constraints, we assume null interaction beyond 200 m (for individuals, Fig. S3a) and between 5000 m (i.e., the size of a grid cell at cohort scale, Fig. S3b) and 9000 m (i.e., radius (α) used to randomly placed offspring from a randomly mature parent). Notice that the null interaction observed beyond 3000 m (Fig. S3b) is only due to parameterization results and is independent of our assumption of "null interaction after 5000 m).

The IPF parameters were fitted to the spatial pattern of the forest stand, as described by the pair correlation function g(r) (Pommerening, 2002). Optimisation was carried using a simulated annealing method (Kirkpatrick *et al.*, 1983) following an algorithm of Metropolis et al. (1953), with fit quality assessed using a least square criterion. For each set of IPF parameters drawn during the optimization process, a point pattern was simulated according to a non-homogeneous Gibbs point process and the pair correlation function was calculated and compared to the observed one.

The IPF parameterization is very sensitive to the way of grouping individual trees into cohorts. As the cohort clustering process transforms inherent spatial properties of trees into inherent spatial properties of cohorts, IPF parameters change to reproduce these new inherent spatial properties. As IPF parameters change with the upscaling, the radius used to randomly placed offspring from a randomly mature parent (α) changes from 200 m (individual tree scale) to 9,000 m (cohort tree scale). As the maximal distance to parameterize the IPF is the size of a grid cell (i.e., 5000 m), we assume null interaction between 5000 m and 9000 m. This parameter mainly affects the maximal distance that offspring are able to reach (Saltré *et al.*, 2009) allowing offspring to potentially across physical dispersal barriers such as mountains (i.e., the Alps) or seas (i.e., the English Channel). However, it does not affect the migration speed because the Gibbs' spatial optimization replaces offspring as a function of species' spatial patterns characteristics whereby optimal distances are not necessarily the maximal distances reachable.

We tested the ability of the IPF to successfully simulate the spatial pattern of a beech forest stand. We compared the spatial pattern simulated using the Gibbs-based migration model to the observed spatial pattern of the beech forest stand. Law et al.,(2009) reviewed main tools used to characterize forest spatial patterns (Rozas *et al.*, 2009) and showed the relevance to use the L-function introduced by Besag (1977) because this function characterises distance between trees throughout several spatial scale of the spatial pattern considered (Stoyan & Penttinen, 2000, Goreaud *et al.*, 2002, Kunstler *et al.*, 2004). L(r) is known to be easy to interpret. Indeed, *L(r)* = 0 (with *r* expressed in metres) under the classical null hypothesis of a complete spatial randomness, corresponding to a Poisson pattern. *L(r)* < 0 indicates that the pattern is regular at range *r*. *L(r)* > 0 indicates that the pattern is clustered at the range *r* (Goreaud *et al.*, 2002). We used this function to make our

comparison. The idea behind the L(r) function is to describe neighbourhood relationship between points based on the average number of points found within the distance r from a typical point (Ilian, 2008).
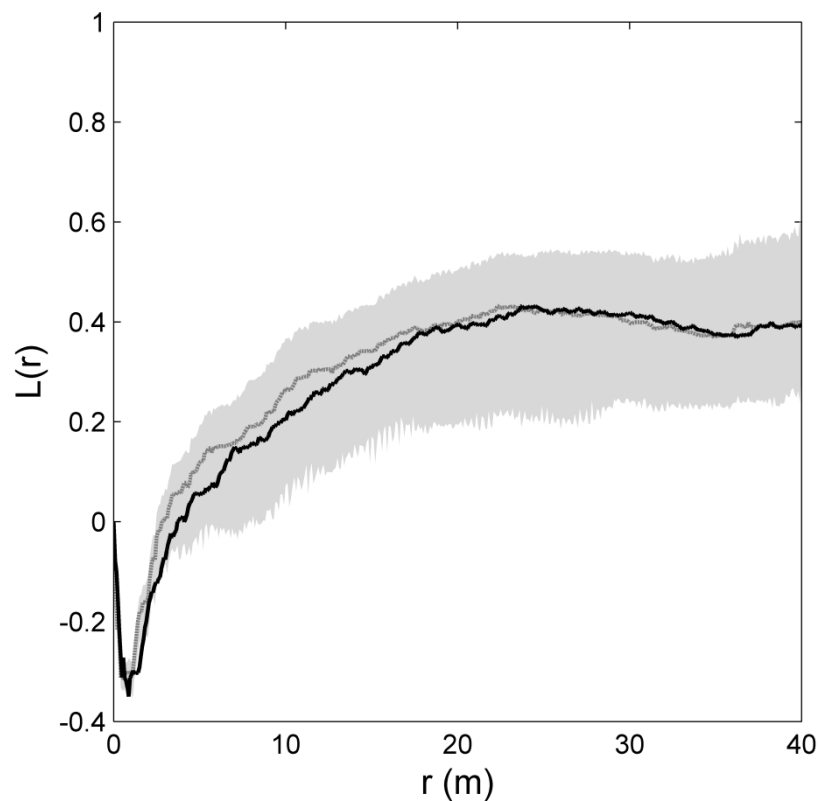
Figure S4. L-function (L(r)) of the observed (black line) and simulated (grey line) European beech pure forest stand. The observed pattern is calculated from an even-aged pure beech stand of 0.4 km², located in the north-eastern Italian pre-Alps on the Cansiglio's Karst Plateau and simulated pattern is calculated from 1000 simulated point pattern with the IPF calibrated at individual scale (Fig. S3a) using a homogeneous Gibbs-process (see detail in Degenhardt & Pofahl, 2000, Stoyan & Pentinnen, 2000). L(r) is calculated for each of the 1000 simulated point pattern so that grey line indicates the median value and grey shade represents the 25th and 75th percentiles. Horizontal axes are the distances r (in metre) between pairs of individuals.

Figure S4 demonstrates a good agreement between simulated and observed beech stand spatial patterns, reproducing the characteristic clustering effect at short distance (<3 m) toward a more regular spatial pattern beyond 10 m.

4. Simulated cohorts' age pattern

a.

b.
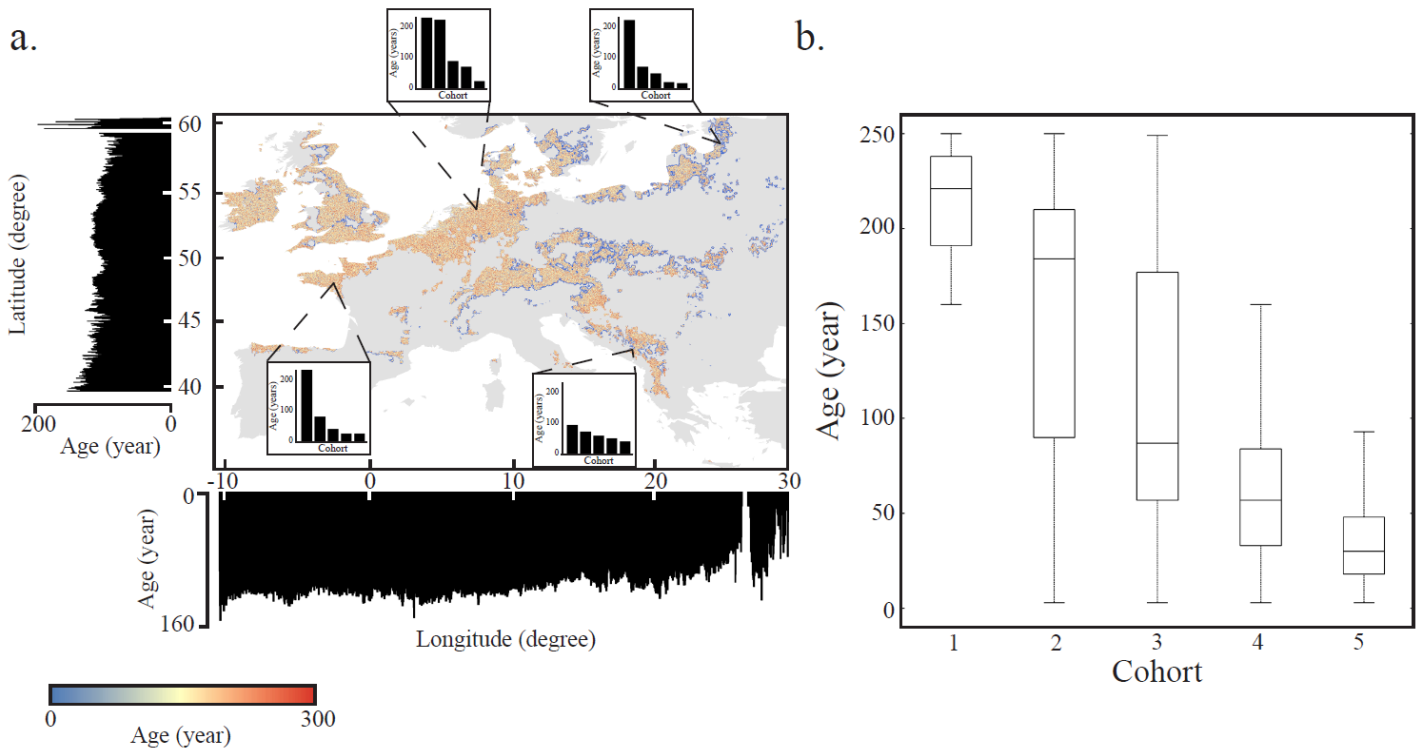
Figure S5. **(a.)** Age distribution (map) of beech cohorts simulated by PHENOFIT coupled to the Gibbs-based migration model according to A1Fi greenhouse gas emission scenario in 2100. Age value (in year) for each grid cell is the averaged value of the age of all cohorts within the cell. Beside each map, the left and bottom panels indicate the distribution across latitude and longitude respectively of the average cohort's age. Each inset (barplot) indicates the age distribution (i.e., the age of each of the five cohorts) for one grid cells among four grid cell randomly chosen across the beech cohort distribution simulated by the model. **(b.)** Boxplot of age distribution of beech cohorts simulated under A1Fi climatic scenario in 2100. Cohorts are sorted as function of their age: Cohort 1 being the oldest and Cohort 5 being the youngest. The central mark is the median, the edges of the box are the 25th and 75th percentiles, and the whiskers extend to the extreme data points not considered as outliers.

Figure S5 shows that age distribution is characterised by youngest cohorts located in newly colonised habitat (Northeastern Europe, Fig. S5 a) and oldest cohorts located in the core of the distribution. However, each grid cell is occupied by cohorts aged from 225 years old (median value, Fig S5b) to 25 years old following 5 age classes.

5. The variation partitioning analysis

Table S1 provides the results of the variation partitioning of expansion and retraction rates among a set of explanatory factors: temperature of the coldest month, mean annual precipitation (both are expressed as grid cell values), land use change (takes 0/1 = no change/change), and integrating a realistic migration/demography (comparing simulation using Gibbs-based model to that using PHENOFIT alone; takes 0/1 = unlimited migration/realistic migration). Values for each explanatory variable correspond to each grid cell, every year, in either expansion areas (blue + black grid cells and black only, Fig. 1 for respectively unlimited and realistic migration) or contraction areas (red only and red + orange grid cell, Fig. 1 for respectively unlimited and realistic migration). Data used in the partial regression analysis correspond to those of colonised and colonisable grid cells (i.e., black and blue pixels in Fig. 1) and extinct grid cells due to climate unsuitability or demographic collapse (i.e., red and orange pixels in Fig. 1). However, due to computational constraints (i.e., 2.5 million of pixels of 25 km2), grid cells were resampled at a 0.5 degree resolution (i.e., 2800 pixels).

Fraction of variation	Adjusted R²		Pvalue	
	expansion	*retraction*	*expansion*	*retraction*
Tmin | (precip. + LUE + migration/demography)	0.089	0.015	0.005	0.005
Precip. | (tmin + LUE + migration/demography)	0.010	0.086	0.005	0.005
LUE | (tmin + precip. + migration/demography)	0.041	0.001	0.005	0.2
Migration/demography |(tmin + precip. + LUE)	0.002	0.052	0.25	0.005
Tmin + precip. + LUE + migration/demography	0.186	0.129	0.005	0.005

Table S1. Result of the variation partitioning analysis. Row 1 to row 4 show the fraction of variation of beech expansion and retraction rates attributable to each explanatory variable conditionally to the other three factors holding constant. Row 5 shows the fraction of the variation attributable to all of the four factors. The significance of the adjusted R² (Pvalue) is tested using F-statistics using 199 permutations of the residuals.

6. Migration rates

Table S2 provides the estimation of minimum, maximum and median expansion / retraction rates of beech in simulations using A1Fi and B2 climate scenarios and the simulation using A1Fi-GRAS climate and land use scenarios. Rates are calculated each ten-year interval, assuming unlimited migration (PHENOFIT) and realistic migration (PHENOFIT + Gibbs-based model). We used the Euclidean Distance function (Spatial Analyst toolbox http://resources.arcgis.com/en/help/main/10.1/index.html#//009z0000001p000000) of ArcGIS© that calculates the Euclidean distance to the closest source for each newly colonised grid-cell (i.e., presence of the species simulated by PHENOFIT + Gibbs-based migration model) and each potentially suitable grid-cell (i.e., presence simulated by PHENOFIT alone). At each *t* year, the closest source is defined either as the closest grid-cell where beech is present (realistic) or potentially present (unlimited) at *t-1* in case of expansion, or at *t+1* in case of contraction.

Migration	A1Fi (2000-2100)		A1Fi-Gras (2000-2100)		B2 (2000-2100)	
	Unlimited	Realistic	Unlimited	Realistic	Unlimited	Realistic
Min	22/22	0/<u>22</u>	22/<u>0</u>	22/<u>22</u>	22/<u>22</u>	22/<u>22</u>
Median	207/<u>284</u>	44/<u>333</u>	138/<u>127</u>	22/<u>328</u>	152/<u>109</u>	22/<u>154</u>
Max	6699/<u>3660</u>	2818/<u>6333</u>	5941/<u>3686</u>	111/<u>6355</u>	5732/<u>1775</u>	90/<u>4186</u>

Table S2. Estimation of minimum (Min), maximum (Max) and median expansion / <u>retraction</u> rates of beech (in m.yrs^{-1}) under the two climate scenarios A1Fi and B2 and the land use change scenario GRAS as a function of two migration scenarios: unlimited migration (climatically suitable habitats simulated with PHENOFIT alone) and realistic migration (colonised habitats simulated by PHENOFIT with migration). Note that with the methodology used, 22 m.yr^{-1} represents the minimal non null rate because one grid-cell is 2.2km x 2.2 km, so that a rate of 22 m.yr^{-1} means just one grid-cell colonised in 100 years.

7. Biological processes limiting fitness
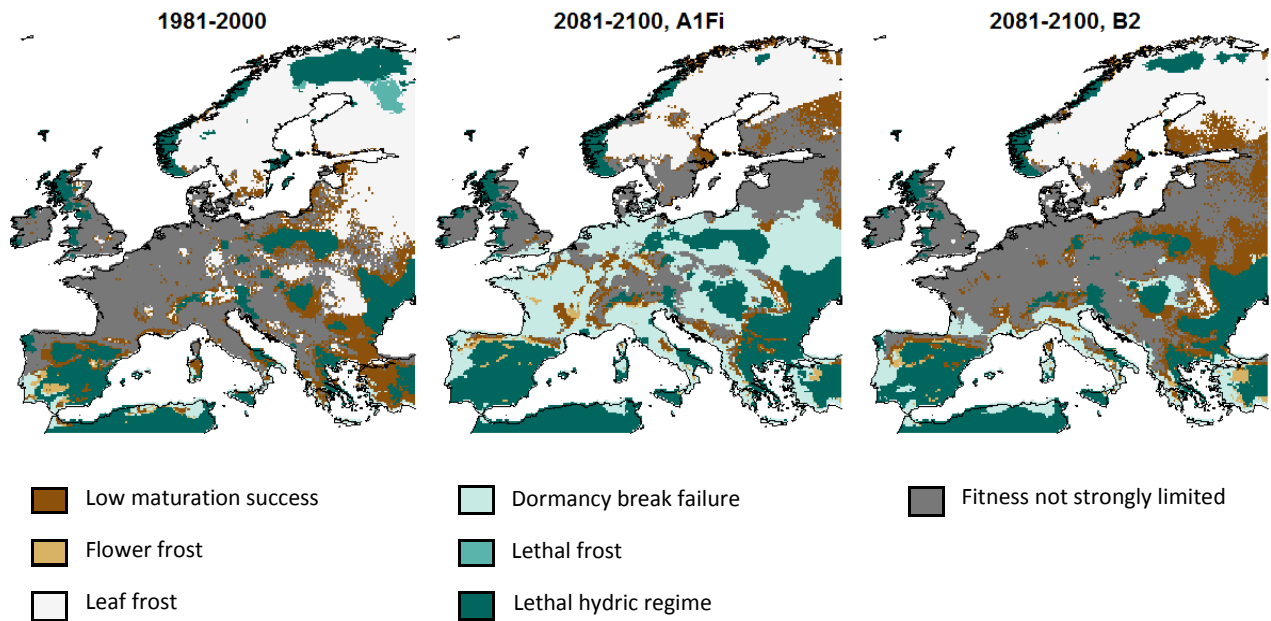
Figure S6. Maps of processes limiting fitness under current (1981-2000) and future climatic conditions (2081-2100, A1Fi and B2 scenarios). The term lethal hydric regime means that the range of precipitation falls either below (500 mm/year) or above the limit of tolerance known for the species (1440 mm/year, http://agriculture.gouv.fr/IMG/pdf/hetre_nov07.pdf)

8. Variations of annual temperature in Europe
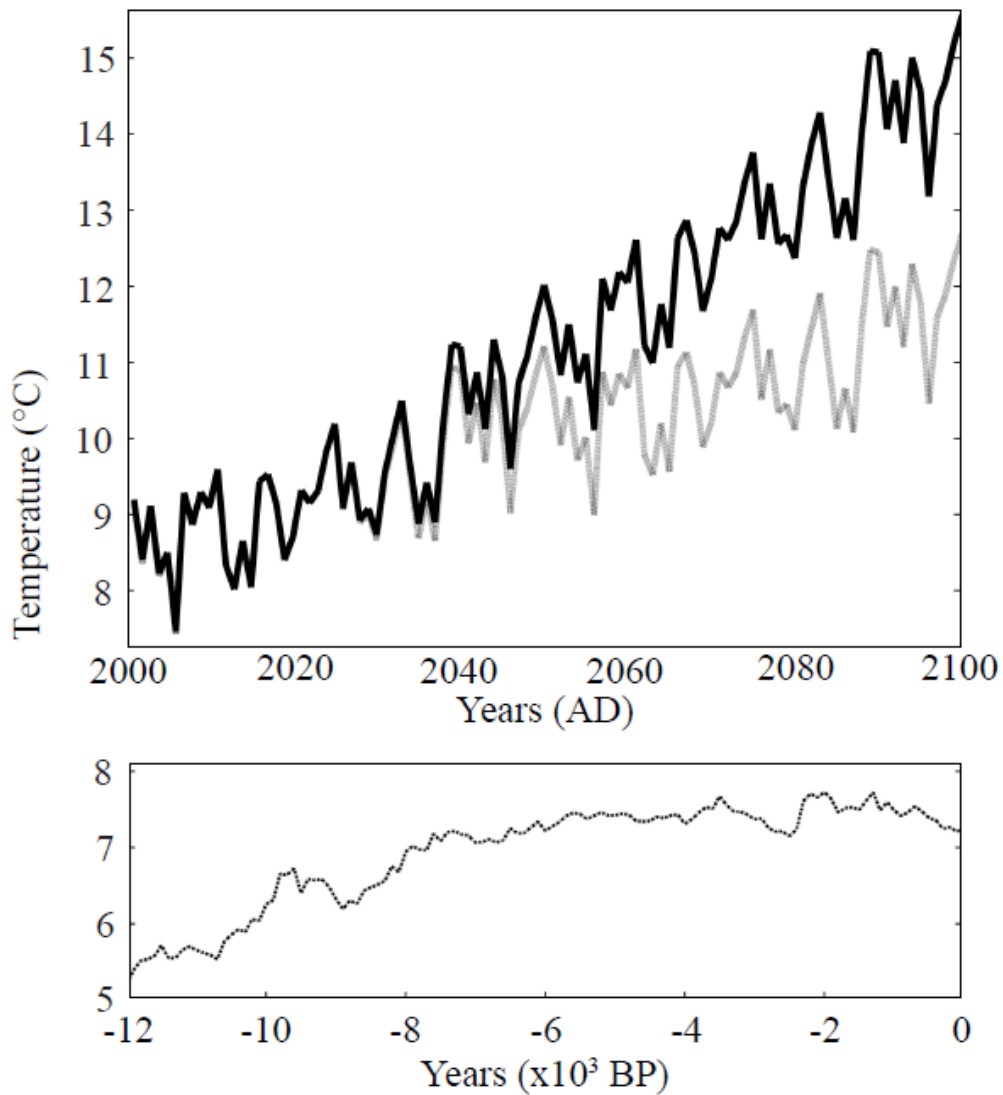
Figure S7. Mean annual temperature in Europe over both the Holocene (from 12000 years BP to present) and the 21st century. The Holocene climate data (dashed plot, lower graph) are the pollen-reconstructed mean annual surface air temperatures from Davis *et al.* (2003), available as a series of gridded fields covering Europe for the last 12000 years at a time step of 100 years and at a spatial resolution of 0.5° x 0.5°. Future climate data are annual climate projections for scenarios of greenhouse gas emission A1Fi and B2 (respectively black and gray curves, upper graph) under the general circulation model HadCM3 (Hadley Centre, United Kingdom, Gordon *et al.,* 2000) at a 10' resolution and obtained from the ATEAM project (Mitchell *et al.*, 2004). Both Holocene and Future data are spatially summarized here by their median value throughout entire Europe at each time step. Note that paleo-precipitation (used in Saltré *et al.,* 2013, which we cannot plot here because still unpublished) do not show major changes compare with future climate scenarios.

9. Future land cover changes under A1Fi-Gras scenario
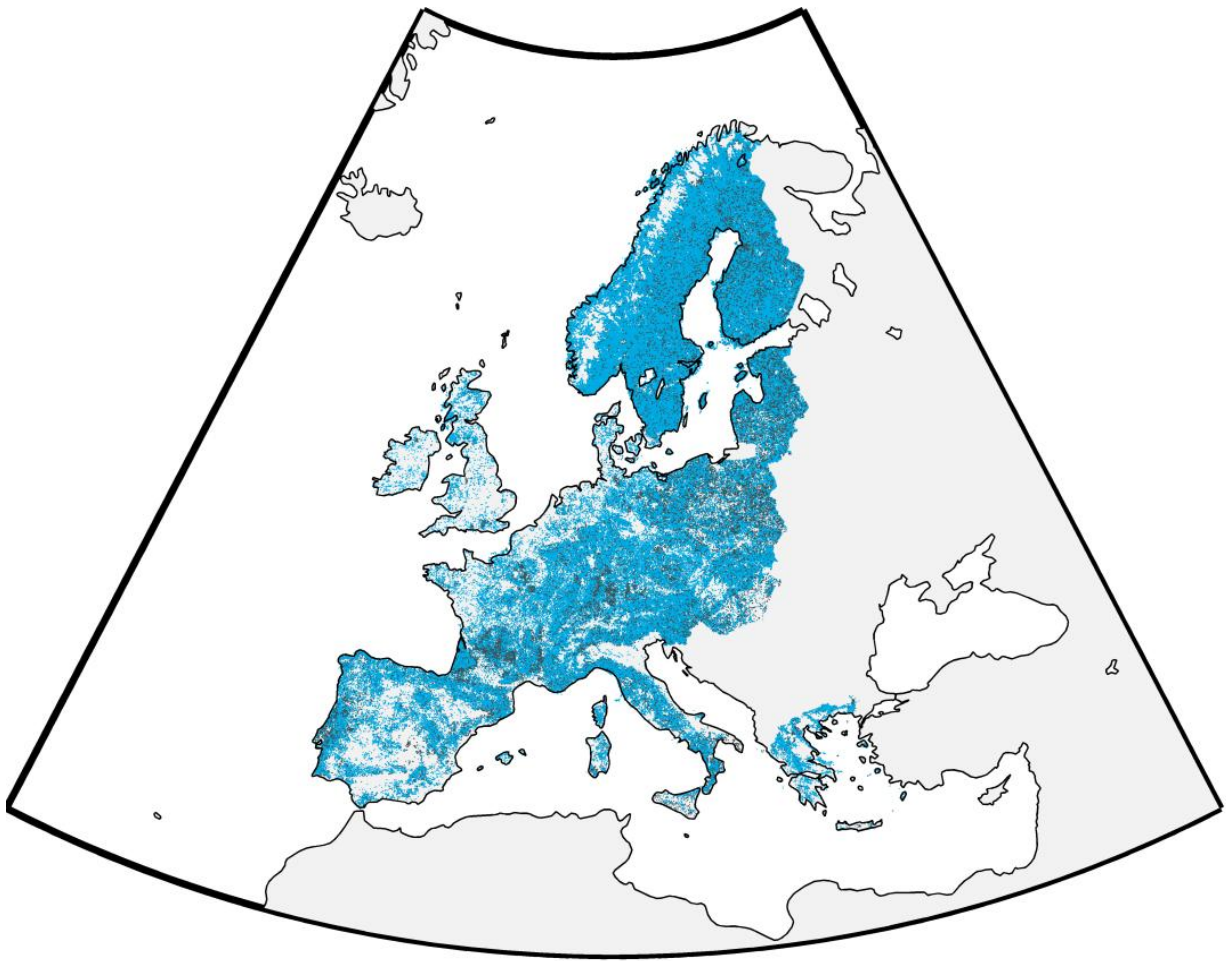
Figure S8. Map of land use changes in Europe between 2000 and 2100 according the ALARM scenario GRAS, downscaled by Meier *et al.* (2012). Grey areas indicate newly emerged forests whereas blue areas indicate areas with no change of land use over the entire period.

References

Besag JE (1977) Comments on Ripley's paper. *Journal of the Royal Statistical Society,* **B 39**, 193-195.

Bohn U, Zazanashvili N, Nakhutsrishvili G (2004) Anwendung und Auswertung der Karte der natürlichen Vegetation Europas / Application and Analysis of the Map of the Natural Vegetation of Europe. In: *Bundesamt für Naturschutz 156: 446 S./pp., 2005* Bonn.

Chuine I, Atauri IGdC, Kramer K, Hänninen H (2013) Plant Development Models. In: *Phenology: An Integrative Environmental Science.* (ed MD S) pp 275-293. Dordrecht, Netherlands, Springer.

Chuine I, Beaubien EG (2001) Phenology is a major determinant of tree species range. *Ecology Letters,* **4**, 500-510.

Chuine I, Cour P, Rousseau DD (1998) Fitting models predicting dates of flowering of temperate-zone trees using simulated annealing. *Plant, Cell and Environment,* **21**, 455-466.

Davis BAS, Brewer S, Stevenson AC, Guiot J, Data Contributors (2003) The temperature of Europe during the Holocene reconstructed from pollen data. *Quaternary Science Reviews,* **22**, 1701-1716.

Degenhardt A, Pofahl U (2000) Simulation of natural evolution of stem number and tree distribution pattern in a pure Pine stand. *Environmetrics,* **11**, 197-208.

Delpierre N, Dufrêne E, Soudani K, Ulrich E, Cecchini S, Boé J, François C (2009) Modelling interannual and spatial variability of leaf senescence for three deciduous tree species in France. *Agricultural and Forest Meteorology,* **149**, 938-948.

Diggle PJ (1985) A kernel method for smoothing point process data. *Applied Statistics,* **34**, 138-147.

Ellenberg H (1996) *Vegetation Mitteleuropas mit den Alpen,* Stuttgart, Ulmer.

Gordon C, Cooper C, Senior CA *et al.* (2000) The simulation of SST, sea ice extents and ocean heat transports in a version of the Hadley Centre coupled model without flux adjustments. *Climate dynamics,* **16**, 147-168.

Goreaud F, Loreau M, Millier C (2002) Spatial structure and the survival of an inferior competitor: a theoretical model of neighbourhood competition in plants. *Ecological modelling,* **158**, 1-19.

Illian J, Penttinen A, Stoyan H, Stoyan D (2008) *Statistical analysis and modelling of spatial point patterns,* West Sussex, England, Wiley.

Jalas J, Suominen J (1964-2010) *Atlas Florae Europaeae,* Helsinki, Finland, The Committee for Mapping the Flora of Europe and Societas Biologica Fennica Vanamo.

Kirkpatrick S, Gelatt CD, Vecchi MP (1983) Optimization by Simulated Annealing. *Science,* **220**, 671-680.

Kunstler G, Curt T, Lepart J (2004) Spatial pattern of beech (Fagus sylvatica L.) and oak (Quercus pubescens Mill.) seedlings in natural pine (Pinus sylvestris L.) woodlands. *European Journal of Forest Research,* **123**, 331-337.

Lahti T, Lampinen R (1999) From dot maps to bitmaps: Atlas Florae Europaeae goes digital. *Acta Botanica Fennica,* **162**, 5-9.

Law R, Illian J, Burslem D, Gratzer G, Gunatilleke CVS, Gunatilleke I (2009) Ecological information from spatial patterns of plants: insights from point process theory. *Journal of Ecology,* **97**, 616-628.

Meier ES, Lischke H, Schmatz DR, Zimmermann NE (2012) Climate, competition and connectivity affect future migration and ranges of European trees. *Global Ecology & Biogeography,* **21**, 164-178.

Metropolis N, Rosenbluth AW, Rosenbluth MN, Teller AH, Teller E (1953) Equation of state calculation by fast computing machines. *Journal of Chemical Physics,* **21**, 1087-1092.

Mitchell TD, Carter TR, Jones PD, Hume M, New M (2004) A comprehensive set of high-resolution grids of monthly climate for Europe and the globe: the observed record (1901–2000) and 16 scenarios (200–2100). *Tyndall Center working paper 55.*

Rozas V, Zas R, Solla A (2009) Spatial structure of deciduous forest stands with contrasting human influence in northwest Spain. *European Journal of Forest Research,* **128**, 273-285.

Saltré F, Chuine I, Brewer S, Gaucherel C (2009) A phenomenological model without dispersal kernel to model species migration. *Ecological modelling,* **220**, 3546-3554.

Saltré F, St-Amant R, Gritti ES, Brewer S, Gaucherel C, Davis BD, Chuine I (2013) Climate or migration: what limited European beech post-glacial colonization? *Global Ecology & Biogeography,* **22**, 1217-1227.

Stoyan D, Penttinen A (2000) Recent Applications of Point Process Methods in Forestry Statistics. *Statistical Science,* **15**, 61-78.

Stoyan D, Stoyan H (1998) Non-homogeneous Gibbs process models for forestry - A Case Study. *Biometrical journal,* **40**, 521-531.